Hybrid Advances 13 (2026) 100648

Contents lists available at ScienceDirect

Hybrid Advances

journal homepage: www.journals.elsevier.com/hybrid-advances

Research Article

Nitrocellulose as a protective dielectric layer for optimized Cu/Ni cryogenic sensors

Moh Toifur [a,*], Yazid Yaakob [b], Okimustava [a], Azmi Khusnani [c], Adi Jufriansah [c], Eko Susanto [d]

[a] Department of Physics Education, Universitas Ahmad Dahlan, Yogyakarta, 55161, Indonesia
[b] Department of Physics, Faculty of Science, Universiti Putra Malaysia, Selangor, 43400, Malaysia
[c] Department of Physics, Universitas Gadjah Mada, Yogyakarta, 55281, Indonesia
[d] Sensor and Transducer Laboratory, Universitas Ahmad Dahlan, Yogyakarta, 55161, Indonesia

ARTICLE INFO

Keywords:
Cryogenic sensor
Copper-nickel
Nitrocellulose coating
Sensitivity
Low temperature

ABSTRACT

Although the potential of Cu/Ni materials and nitrocellulose coatings for cryogenic temperature sensors is acknowledged, a significant knowledge gap persists regarding the quantitative impact of nitrocellulose coating thickness variations on the electrical and thermal performance of Cu/Ni-based sensors at cryogenic temperatures. This work investigates the protective function of nitrocellulose (NC) layers in Cu/Ni-based cryogenic temperature sensors, emphasizing the impact of coating thickness (0–0.74 mm) on thermal and electrical performance. The sensors were fabricated by electroplating nickel onto copper substrates, followed by NC spray coating. Key parameters, including voltage range, response time, activation energy, hysteresis loss, and absolute sensitivity, were evaluated over the temperature range of 0 °C to −160 °C. The results show that NC layers provide both mechanical and chemical protection while modulating heat transfer and charge transport. An optimal thickness (0.30–0.43 mm) balances protection, high sensitivity, and rapid thermal response, with a peak voltage range of 0.17 V and increased activation energy. Thicker layers (>0.43 mm) improve cryogenic sensitivity (>6 Ω/°C at −160 °C) but reduce performance at higher temperatures. A multivariate logarithmic regression model accurately predicts sensitivity from physical parameters, enabling design optimization. These findings highlight NC thickness control as a practical approach to enhancing durability and sensitivity in cryogenic sensor applications.

1. Introduction

Accurate temperature measurement under cryogenic conditions is essential for many modern technologies operating at extremely low temperatures. Applications such as superconducting systems, liquefied gas storage and transportation, biomedical cryopreservation, and aerospace instrumentation require reliable temperature monitoring to ensure operational stability and experimental accuracy. Consequently, the development of robust cryogenic temperature sensors with high sensitivity, stability, and fast thermal response has become an important research focus in recent years [1–8].

Conventional cryogenic temperature sensors commonly employ platinum because of its stable and well-characterized resistance–temperature relationship. However, the high cost of platinum and the increasing demand for compact and cost-effective sensing devices have motivated the exploration of alternative materials. Copper (Cu) and nickel (Ni), in alloy or bilayer form, have attracted attention for their favorable electrical conductivity, mechanical robustness, and relatively low cost [9–11]. In particular, Cu/Ni bilayer systems exhibit tunable resistivity and stable electrical behavior at low temperatures. Moreover, Cu/Ni sensing structures can be fabricated via electroplating, enabling the simple, scalable production of cryogenic sensors [12].

Despite these advantages, Cu/Ni-based sensing materials remain vulnerable to oxidation and corrosion. The formation of oxide layers such as CuO, Cu_2O, and NiO can introduce additional resistive barriers that alter the intrinsic resistance–temperature (R–T) characteristics and reduce measurement accuracy [13], [14]. Corrosion processes may also induce morphological degradation, including pitting, microcracks, and localized thinning of the sensing layer, which reduces the effective conductive cross-section and increases electron scattering [15–18]. These effects can lead to thermal hysteresis and decreased sensor stability during repeated cooling–heating cycles. Therefore, protective

* Corresponding author.
E-mail addresses: toifur@mpfis.uad.ac.id (M. Toifur), yazidakob@upm.edu.my (Y. Yaakob), okimustava@pfis.uad.ac.id (Okimustava), azmikhusnani@mail.ugm.ac.id (A. Khusnani), adijufriansah@mail.ugm.ac.id (A. Jufriansah), ekosusanto@staff.uad.ac.id (E. Susanto).

https://doi.org/10.1016/j.hybadv.2026.100648
Received 5 February 2026; Received in revised form 17 March 2026; Accepted 26 March 2026
Available online 20 April 2026

coatings are commonly applied to maintain the structural integrity and electrical stability of metal-based temperature sensors [19–22].

Polymer-based coatings are widely used in sensor technologies to enhance environmental stability and corrosion resistance. In addition to providing chemical protection, polymer coatings may also influence sensor performance by modifying heat transfer between the sensing layer and the surrounding environment. Previous studies have reported that dielectric or polymer coatings can alter thermal response by introducing additional thermal resistance and modifying interfacial charge-transport mechanisms. In this context, coating thickness becomes a key parameter because it determines the level of thermal insulation and the interaction between the sensing material and the external environment. Variations in coating thickness have been shown to influence response time significantly, signal amplitude, and temperature sensitivity of sensors due to changes in heat transfer pathways and interfacial transport processes [23], [24].

Nitrocellulose (NC) resin represents a promising protective material due to its dielectric properties, optical transparency, chemical stability, and ease of deposition [25]. These characteristics allow NC to function as a protective layer without introducing significant chemical reactivity with the metallic sensing element. However, a dielectric polymer coating can alter the sensor's thermal response by introducing additional thermal resistance and affecting interfacial charge-transport processes. Consequently, variations in NC coating thickness may affect key sensor parameters, including voltage response, response time, activation energy, hysteresis behavior, and temperature sensitivity.

Although polymer coatings have been widely investigated in various sensing systems, systematic studies focusing on nitrocellulose coatings in Cu/Ni-based cryogenic temperature sensors remain limited, particularly regarding the quantitative relationship between coating thickness and sensor performance. A clearer understanding of how NC layer thickness influences heat transfer, electrical transport, and signal stability is therefore required for optimizing protective coatings in cryogenic sensing applications.

In this study, we systematically investigate the influence of nitrocellulose coating thickness on the performance of Cu/Ni-based cryogenic temperature sensors. The NC coating thickness was varied from 0 to 0.74 mm, and its effects on voltage range, response time, activation energy, hysteresis loss, and absolute sensitivity were evaluated over the temperature range from 0 °C to −160 °C. The novelty of this work lies in establishing a quantitative relationship between NC coating thickness and key performance parameters of Cu/Ni cryogenic sensors. In addition, a multivariate regression model is proposed to correlate sensor sensitivity with underlying physical parameters, providing further insight into the role of polymer protective layers in cryogenic sensing systems. From a physical perspective, the coating thickness controls both thermal resistance and interfacial electron transport, thereby determining the dynamic and electrical response of the sensor under cryogenic conditions.

2. Experimental method

2.1. Preparation of Cu/Ni/NC samples

The fabrication of the Cu/Ni/NC sensor involved several main stages, including Cu substrate preparation, Cu/Ni electroplating, and NC coating. The detailed preparation procedure is illustrated in the flowchart presented in Fig. 1.

On the substrate preparation, a nickel plate (1.5 cm × 10 cm × 0.1 mm) was prepared as the coating source. A commercial copper substrate (PCB) was machined into a square-wave pattern with dimensions of 108 mm × 2 mm × 70 μm. Both surfaces were sequentially polished with a soft cloth using Autosol metal polish (SM583), then with toothpaste, until a reflective finish was achieved. The substrates were rinsed with distilled water, followed by 95 % ethanol, and cleaned in an ultrasonic bath for 15 min. After drying, the Cu plate was weighed using an Ohaus PR223/E analytical balance.

On the Cu/Ni electroplating, Cu/Ni samples were fabricated in an electroplating reactor, with a nickel plate serving as the anode and a copper substrate as the cathode, separated by 4 cm. Both electrodes were immersed in an electrolyte containing $NiSO_4$ (260 g), $NiCl_2$ (60 g), H_3BO_3 (40 g), and 150 mL of distilled water, maintained at 60 °C. Electroplating was conducted at a constant voltage of 4.5 V for 5 min. Fig. 2 presents the schematic of the sample and the resulting plated structure.

For the NC coating, before spraying, each sample was weighed and its sheet resistivity measured. The Cu/Ni substrate surface was then uniformly coated with Enzo 5240 NC using a spray pressure of 1.2 MPa. The coated sample was dried for 15 min to ensure complete solvent evaporation (Fig. 2a), after which its weight and sheet resistivity were remeasured. This procedure was repeated up to five cycles, with weighing and resistivity measurements performed after each coating step.

2.2. Determination of Ni and NC layer thicknesses

The Cu/Ni and Cu/Ni/NC samples were weighed using an Ohaus PR223/E analytical balance to obtain the masses of the Cu substrate, the Cu/Ni sample, and the Cu/Ni/NC sample. The thickness of the Ni layer thickness was calculated indirectly determined by the gravimetric method according to the following equation [26]:

$$t_{Ni} = \frac{m_{Cu/Ni} - m_{Cu}}{\rho_{Ni} A}, \tag{1}$$

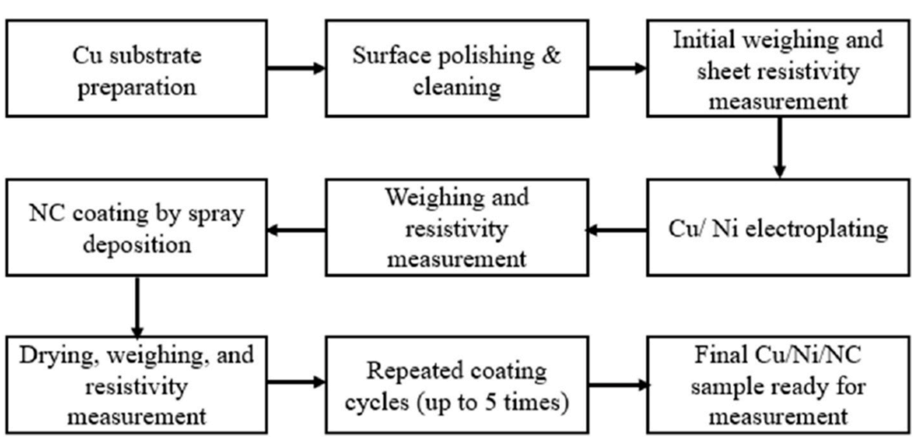

Fig. 1. Flowchart of the preparation process of the Cu/Ni/NC samples.

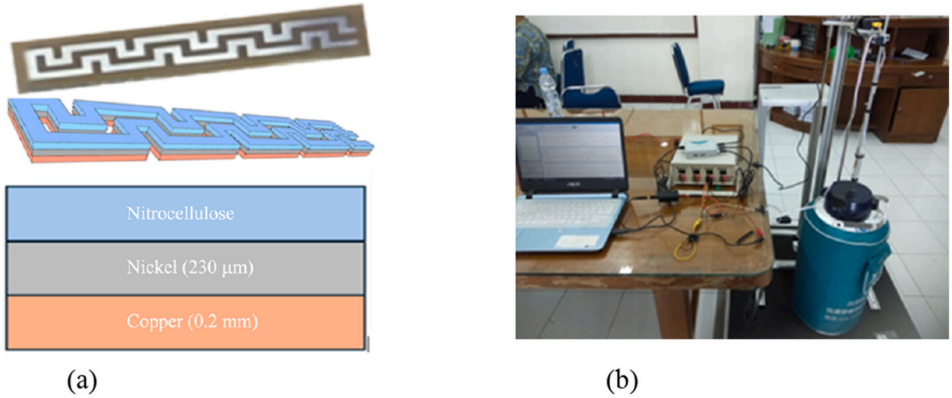

Fig. 2. (a) Schematic of the sample sketch, perspective view, and Cu/Ni sample, and (b) Low-temperature measurement research apparatus.

where t_{Ni} is the thickness of the Ni layer, $m_{\mathrm{Cu/Ni}}$ is the mass of the Cu/Ni sample, m_{Cu} is the mass of the Cu substrate, ρ_{Ni} is the density of nickel (8.908 $\mathrm{gcm^{-3}}$), and A is the deposition area in $\mathrm{cm^2}$. Similarly, using the mass values of the Cu/Ni sample and the Cu/Ni/NC sample, along with the density of NC, the thickness of the NC layer was determined indirectly using the gravimetric method according to the following equation:

$$t_{\mathrm{NC}} = \frac{m_{\mathrm{Cu/Ni/NC}} - m_{\mathrm{Cu/Ni}}}{\rho_{\mathrm{NC}} A} \quad (2)$$

where t_{NC} is the thickness of the NC layer, $m_{\mathrm{Cu/Ni/NC}}$ is the mass of the Cu/Ni/NC sample, $m_{\mathrm{Cu/Ni}}$ is the mass of the Cu/Ni sample, ρ_{NC} is the density of nitrocellulose (1.23 $\mathrm{gcm^{-3}}$), and A is the deposition area in $\mathrm{cm^2}$.

2.3. Determination of sheet resistivity

The sheet resistivity (R_s) of the Cu/Ni and Cu/Ni/NC samples was measured using a four-point probe system (JG-ST2258C). A higher R_s value for the Cu/Ni sample ($R_{s\mathrm{Cu/Ni}}$) compared to that of the pure Cu substrate ($R_{s\mathrm{Cu}}$) confirms successful Ni electroplating, as the resistivity of pure Ni (6.99×10^{-8} Ω m) exceeds that of Cu (1.68×10^{-8} Ω m) according to standard reference values. Likewise, if the R_s of the Cu/Ni/NC sample approaches infinity (or is detected as non-conductive), it indicates successful application of the NC coating, since NC is an electrically insulating material.

2.4. Morphology surface

Surface morphology was characterized using a JEOL JCM-7000 scanning electron microscope (SEM). SEM images of the Cu/Ni and Cu/Ni/NC film surfaces were obtained to examine the morphology, grain distribution, and surface uniformity of the deposited films.

2.5. Measurement of voltage, temperature, and current

The Cu/Ni/NC sensor, coupled with a TCA-BTA thermocouple, was gradually immersed in a Dewar flask containing liquid nitrogen at a controlled descent rate of 1.07 cm $\mathrm{min^{-1}}$ (Fig. 2b). Measurements were acquired at a sampling rate of 1 sample per second. During immersion, the thermocouple temperature decreased from 0 °C to −165 °C, corresponding to the lowest measurable temperature in liquid nitrogen. The sensor was then steadily withdrawn until the temperature returned to 0 °C.

Through both cooling and warming cycles, the sensor's output voltage was recorded using a Vernier VP-BTA voltage probe. At the same time, the corresponding current was measured with a Vernier DCP-BTA current probe. Voltage data were analyzed to evaluate the sensor's thermal responsiveness. A strong correlation between voltage and temperature confirmed proper operation and high thermal sensitivity of the Cu/Ni/NC sensor [27–29].

The voltage range was obtained by calculating the difference between the sensor voltage at the temperature of 0 °C and the temperature of −160 °C:

$$\Delta V = V_{0^\circ\mathrm{C}} - V_{-160^\circ\mathrm{C}}, \quad (3)$$

where ΔV is the voltage range of the sensor, V_0 is the sensor voltage at 0 °C, and V_{-160} is the sensor voltage at −160 °C. The response time was determined from the transient voltage–time response using Gaussian fitting. In this approach, the response time corresponds to the full width at half maximum (FWHM) of the fitted Gaussian function, a method commonly used in the dynamic characterization of temperature sensors to describe the temporal width of the sensor response during the cooling process [30]:

$$y(t) = Ae^{-\frac{(t-t_0)^2}{2\sigma^2}} \quad (4)$$

where $y(t)$ represents the sensor signal (voltage), A is the maximum amplitude, t_0 is time at the peak position, and σ is the temporal standard deviation. The temporal width of the response was calculated using the full width at half maximum (FWHM), given by $t_{resp} = 2.355\sigma$ [31]. The uncertainty of the response time was obtained by error propagation from the fitting parameter σ, yielding $s_{t_{resp}} = 2.355\, s_\sigma$.

The activation energy was determined using the Arrhenius relationship between electrical conductivity and temperature [32], which describes thermally activated charge transport in conductive materials:

$$\sigma = \sigma_0 e^{E_a/kT}, \quad (5)$$

where σ is the electrical conductivity, σ_0 is the pre-exponential factor, E_a is the activation energy (J), k is the Boltzmann constant (1.380649×10^{-23} J/K), and T is the absolute temperature (K). The electrical conductivity can be determined from the resistance, the length of the sample, and the cross-sectional area according to the following equation:

$$\sigma = \frac{1}{\rho} = \frac{L}{RA}, \quad (5)$$

where σ is the electrical conductivity, R is the resistance of the Cu/Ni or Cu/Ni/NC sensor, L is the sensor length (108 mm), and A is the cross-sectional area of the sensor (432 $\mathrm{mm^2}$). By taking the natural logarithm of Eq. (5), the linear form is expressed as:

$$\ln\sigma = \ln\sigma_0 + \left(\frac{10^3 E_a}{k}\right)\frac{1}{10^3 T}. \quad (6)$$

where σ is the electrical conductivity, σ_0 is the pre-exponential factor, E_a

is the activation energy (J), k is the Boltzmann constant, and T is the absolute temperature (K). By plotting $\ln\sigma$ as a function of $1/(kT)$, the activation energy can be determined from the slope of the linear Arrhenius plot [33]:

$$E_a = \frac{Bk}{10^3}\ (\text{joule}). \tag{7}$$

where E_a is the activation energy (J) and B is the slope of the linear regression obtained from the plot of $\ln\sigma$ versus $1/(kT)$. A sensor with a lower activation energy E_a allows current to flow more easily. The smaller the E_a, the easier it is for charge carriers to move through the material.

Hysteresis loss was determined by calculating the maximum resistance difference between the heating and cooling curves at the same temperature, which is a commonly used method for evaluating sensor hysteresis [34], [35]:

$$H_L = (V_c - V_h)_{\max}, \tag{8}$$

where HL is the hysteresis loss, V_c is the sensor voltage during the cooling process, and V_h is the sensor voltage during heating. The electrical resistance of the sensor was calculated from the measured voltage and applied current using Ohm's law:

$$R = \frac{V}{I} \tag{9}$$

where R is the electrical resistance of the sensor, V is the measured voltage, and I is the applied current. The resistance–temperature relationship was then fitted using an exponential function:

$$R(T) = A - Be^{CT} \tag{10}$$

where R is the resistance, T is the temperature, and A, B, and C are fitting constants. The absolute sensitivity (S) was obtained from the slope of the curve described by Eq. (10), which represents the rate of change of the sensor output with respect to temperature, following the method proposed by Haris and Lu [36], [37], [38]:

$$S(T) = \frac{dR(T)}{dT} = -De^{mT} \tag{11}$$

where S represents absolute sensitivity, D and m are constants, with T being the temperature.

3. Results and discussion

Table 1 presents the physical properties of the Cu substrate before and after Ni coating, including sheet resistivity, mass, and estimated Ni film thickness. The table also includes the range of NC protective layer thicknesses applied for subsequent performance evaluation of the cryogen, as well as the calculated Ni and NC layer thicknesses obtained from Eqs. (1) and (2).

3.1. Surface morphology

Fig. 3 presents the SEM images of the Cu/Ni film and the Cu/Ni film coated with nitrocellulose (NC), each observed at two different locations to evaluate the surface morphology and its spatial uniformity.

Fig. 2a and b shows the SEM images of the Cu/Ni film before and after nitrocellulose (NC) coating. The uncoated Cu/Ni surface exhibits a relatively compact morphology with visible grain structures characteristic of electroplated metallic films. After NC deposition (Fig. 2c and d), the surface appears covered by a continuous polymer layer that partially smooths the underlying metallic features while maintaining good adhesion to the substrate. The NC layer forms a relatively uniform coating over the Cu/Ni surface, indicating effective coverage of the sensing element. This morphological modification suggests that the NC coating alters the effective conduction pathways at the film surface and introduces an additional interfacial layer between the sensing element and the surrounding environment. From a thermal perspective, the presence of the polymer coating may increase the effective thermal resistance, thereby influencing heat transfer dynamics between the sensing layer and the cryogenic medium. Consequently, the NC layer may affect the electrical transport behavior of the sensor, which is consistent with the observed changes in activation energy and response characteristics discussed in the following sections.

3.2. Temperature and sensor voltage response

Fig. 4 shows the transient voltage response of Cu/Ni/NC-based cryogenic temperature sensors with NC coating thicknesses ranging from 0 to 0.74 mm during cooling from 0 °C to −160 °C and subsequent warming to 0 °C. All sensors responded measurably to temperature changes, exhibiting distinct voltage ranges and rates of change [39], [40]. The uncoated sensor (S0) displayed the fastest voltage drop during cooling, indicating an immediate thermal response. In contrast, NC-coated sensors exhibited a pronounced thermal lag, with thicker coatings (S4, S5) producing slower voltage decreases. This behavior is attributed to the low thermal conductivity and additional thermal mass of the NC layer.

Under steady-state low-temperature conditions near −160 °C, all sensors exhibited a minimum voltage of 0.50–0.52 V, indicating that NC thickness has only a minor effect on the equilibrium response. In contrast, during transient phases (cooling and warming), thicker NC layers markedly slowed the voltage dynamics. This behavior is consistent with previous findings that polymer coatings can alter the dynamic thermal response of cryogenic sensors by increasing thermal resistance and capacitance [41]. A quantitative analysis of the transient sensor response, including response time and voltage range, is presented in Sections 3.3 and 3.4.

3.3. Response time analysis

The response time was defined as the full width at half maximum (FWHM) of the Gaussian-fitted voltage–time response. Fig. 5 shows the relationship between NC thickness and sensor response time, indicating that the NC coating significantly influences the sensor's thermal response characteristics.

From Fig. 5, the uncoated sensor exhibited the fastest response (∼277 s), reflecting minimal thermal resistance and direct heat transfer to the active sensing layer.

Similar trends have been reported for Cu/Ni-based sensors, where response time, derived from voltage–time curves during liquid nitrogen vapor cooling [42], [43], increases in the presence of thermal insulation layers, such as NC. As NC thickness increased to 0.10 mm and 0.30 mm, the response time rose markedly, peaking at ∼308 s at 0.30 mm. This indicates that the NC layer acts as a thermal barrier, impeding heat transfer from the environment to the Cu/Ni surface and thereby delaying the sensor's thermal equilibration [23], [44].

Interestingly, increasing the NC thickness to 0.43 mm, 0.57 mm, and 0.74 mm gradually reduced the response time. This behavior may result from morphological changes in the NC layer, such as decreased packing

Table 1
Physical properties of Cu before and after Ni coating.

No.	Measured parameter	Value
1	Sheet resistivity of Cu	(1040 ± 0,004) $\times 10^{-3}$ Ω/sq
2	Sheet resistivity of Cu/Ni	(3,81 ± 0,02) $\times 10^{-3}$ Ω/sq
3	-voltage Mass of Cu plate	(2936,08 ± 0,05) mg
4	Mass of Cu/Ni plate	(2953,16 ± 0,05) mg
5	Mass of Ni film	(17,08 ± 0,07) mg
6	Thickness of Ni film	(128,57 ± 0,71) μm
7	Thickness of NC film	0 up to 0.74 mm

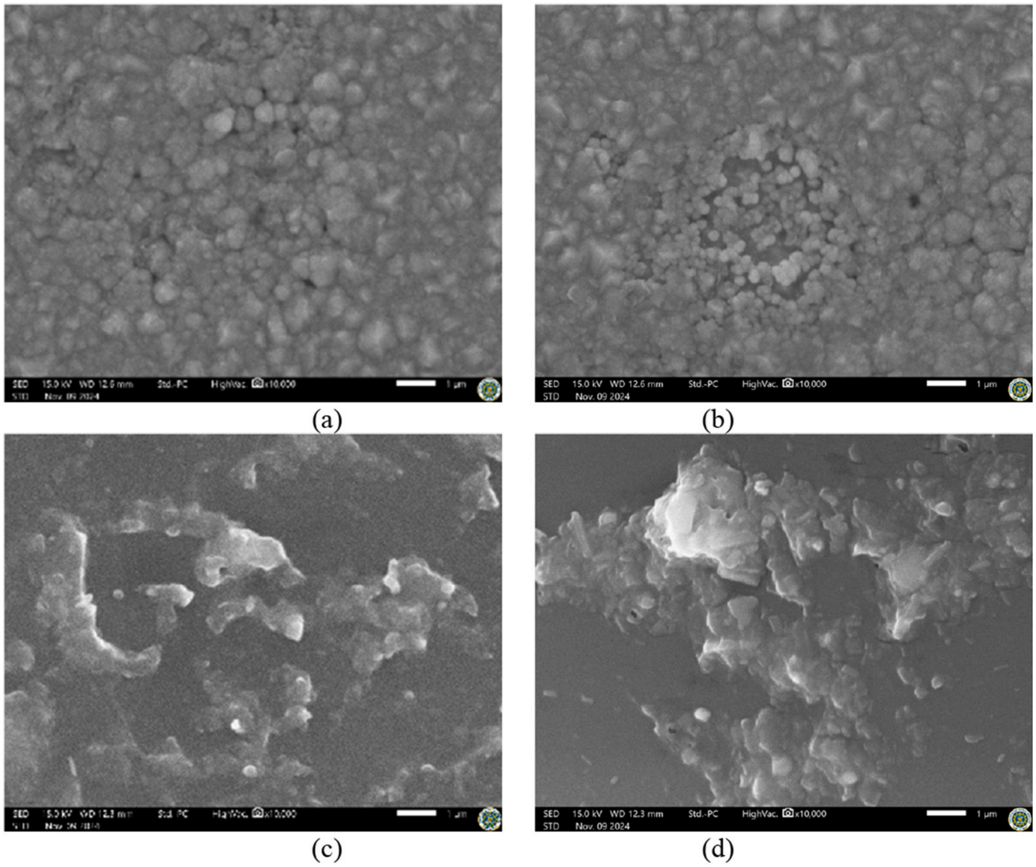

Fig. 3. SEM images of Cu/Ni (a, b) and Cu/Ni/NC (c, d) surfaces taken at two different locations (× 10,000, scale bar 1 μm).

density or micro-defect formation, that facilitate more efficient thermal exchange compared to the intermediate thickness range [45], [46].

3.4. Voltage range analysis

Fig. 6 presents the relationship between the sensor's voltage range and NC layer thickness. The voltage range, defined as the difference between the maximum and minimum output voltages over a temperature range from 0 °C to −160 °C, was evaluated for different NC thicknesses.

As shown in Fig. 6, the sensor output varied systematically with the protective layer thickness [24], [47]. The uncoated sensor (S0) exhibited the narrowest range, whereas increasing the NC thickness to 0.10 mm and 0.30 mm broadened it, reaching a maximum of approximately 0.17 V at 0.30 mm. This enhancement is likely due to improved surface stability and reduced electrode interface noise provided by the thin dielectric layer, which sharpens the signal response under cryogenic conditions.

However, increasing the NC layer to 0.45 mm led to a sharp decline in the voltage range, a trend that persisted with thicker coatings. This behavior suggests that excessive insulation introduces parasitic resistance, hindering charge transport at low temperatures. The diminished voltage dynamics at greater NC thicknesses further indicate reduced sensor responsiveness, likely due to interfacial thermal and electrical barriers imposed by the thick polymer layer.

These findings indicate an optimal NC thickness of approximately 0.30 mm, at which the sensor provides adequate protection and high electrical responsiveness. Beyond this point, excessive coating degrades voltage output, compromising accurate signal interpretation in cryogenic sensing applications.

3.5. Effect of NC thickness on activation energy

Arrhenius-type plots of ln σ versus $1/1000\,T$ for Cu/Ni sensors with varying NC coating thicknesses (Fig. 7a) reveal a systematic effect of the protective layer on electrical conductivity.

The uncoated sensor exhibits the highest ln σ values over the entire temperature range, indicating minimal obstruction to charge transport in the absence of NC. In contrast, NC-coated sensors display a progressive downward shift in conductivity curves, with thicker layers showing more pronounced reductions. This trend suggests that the NC film introduces an additional barrier to carrier mobility, attributed to its insulating character and the increased thermal resistance at greater thickness [48]. Despite all samples maintaining a linear ln σ–temperature relationship consistent with Eq. (6), slope variations reflect corresponding changes in activation energy for electrical conduction [49].

The variation in activation energy with NC coating thickness is shown in Fig. 7b. As discussed in subsection 3.3, increasing the NC coating thickness modifies the sensor's thermal response by introducing an additional insulating layer that influences heat transfer and interfacial transport. At relatively thin coating thicknesses (≤0.15 mm), the NC layer may remain thin, allowing the underlying Cu/Ni surface to continue influencing charge transport. Under these conditions, electrons can interact more directly with the metallic layer, and charge transport may occur with relatively small energy barriers via thermally assisted conduction and electron scattering, resulting in a lower activation energy [50], [51]. When the NC thickness approaches ∼0.30 mm, the polymer layer becomes more continuous and uniformly covers the Cu/Ni surface. This continuous layer increases the effective transport barrier at the Cu/Ni–NC interface, thereby restricting charge-carrier mobility and increasing interfacial resistance. Consequently, the activation energy reaches its maximum, suggesting that the conduction

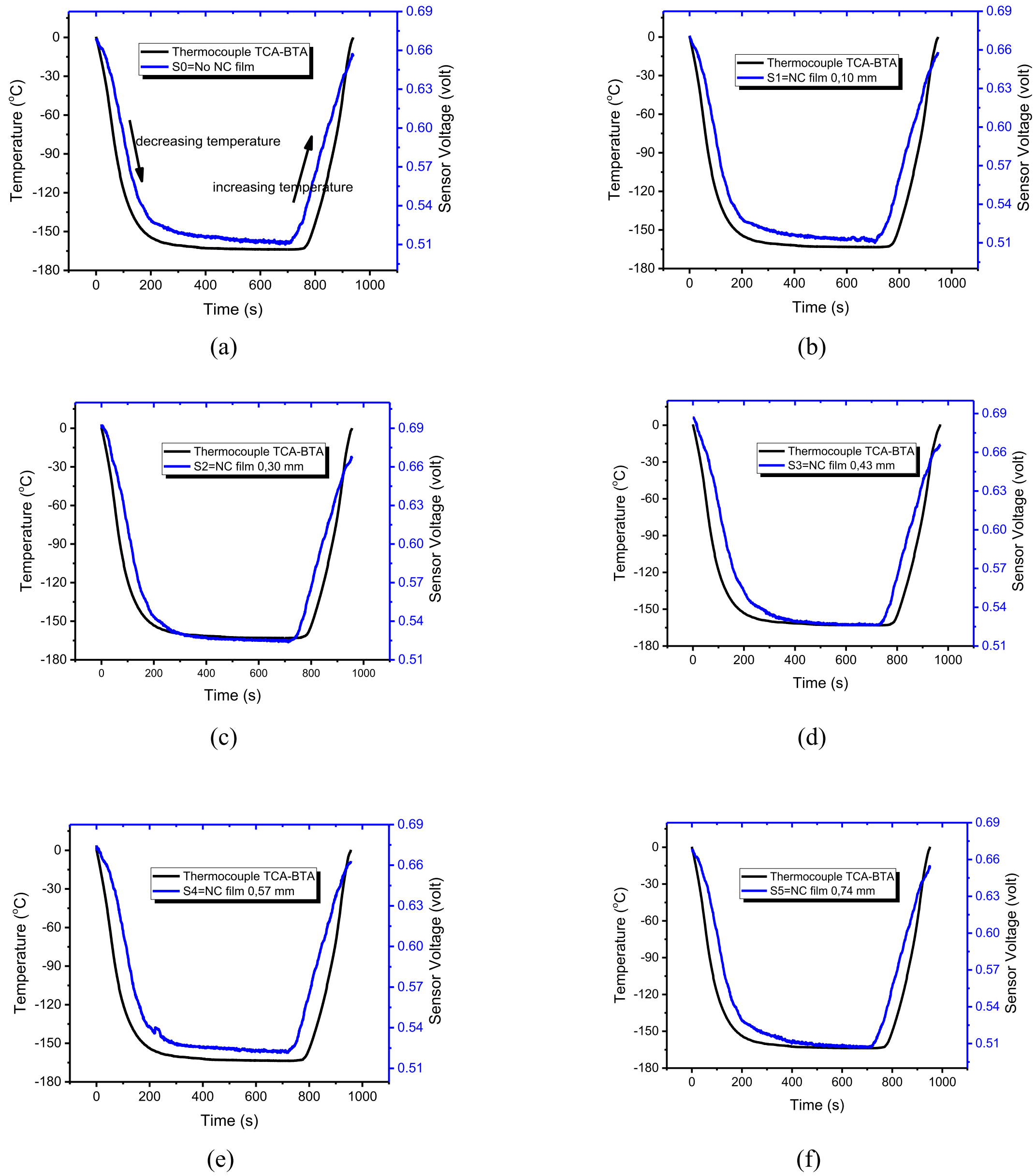

Fig. 4. Transient voltage response of Cu/Ni sensors with different NC coating thicknesses during cooling and heating cycles between 0 °C and −160 °C.

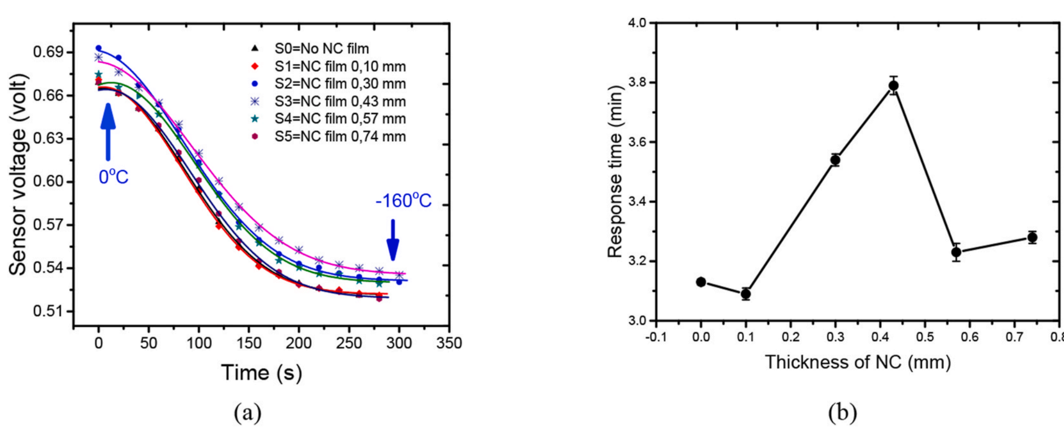

Fig. 5. (a) Sensor voltage during the measurement of liquid nitrogen temperature from 0 °C to −160 °C and (b) Response time for various NC coating thicknesses.

process is increasingly influenced by the insulating polymer layer [52]. For thicker coatings (>0.45 mm), the activation energy decreases

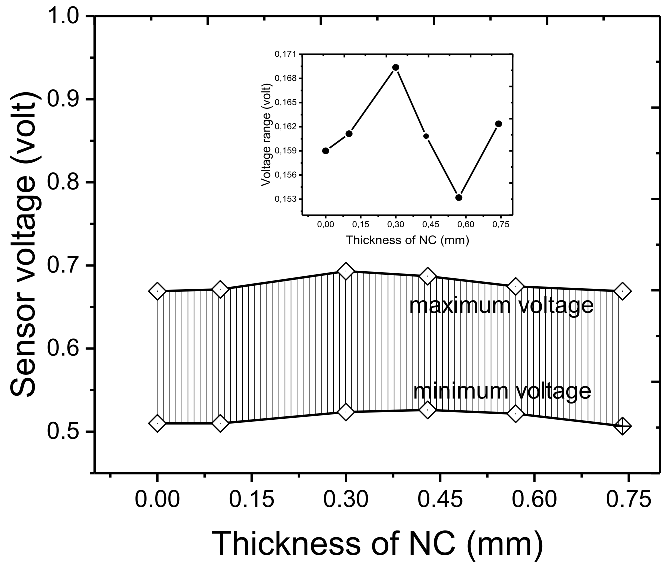

Fig. 6. Characteristics of maximum and minimum sensor voltage and voltage range.

slightly before increasing again at the largest thickness. This behavior suggests that the effective transport barrier within the polymer layer does not increase monotonically with thickness. Variations in the internal structure of the polymer layer may locally modify the transport barrier, thereby contributing to the observed reduction in activation energy.

3.6. Effect of NC thickness on hysteresis behavior

Fig. 8 presents the resistance–temperature characteristics of Cu/Ni sensors coated with NC layers of varying thicknesses, recorded during both heating and cooling cycles. Each curve exhibits a distinct hysteresis loop, reflecting differences in resistance at the same temperature between the heating and cooling phases. This hysteresis behavior indicates the presence of thermal lag in the sensor system, which contributes to the observed hysteresis loss, a critical parameter for assessing the reversibility and dynamic accuracy of temperature sensors.

Hysteresis loss increased progressively as the NC thickness was raised from 0.00 mm to 0.43 mm, indicating that the protective layer induces thermal inertia. This behavior is attributed to the insulating nature of NC, which slows heat transfer between the environment and the sensing element. The uncoated sensor (0.00 mm) exhibited the smallest hysteresis loss, indicating a rapid and nearly reversible thermal response. In contrast, at a thickness of 0.43 mm, hysteresis became more pronounced, reflecting greater resistance deviation between heating and cooling cycles.

A sharp and unexpected peak in hysteresis loss was observed at a thickness of 0.57 mm, coinciding with the maximum separation between the heating and cooling curves. This indicates a critical threshold beyond which the NC coating degrades sensor responsiveness, likely due to pronounced heat retardation and internal structural relaxation within the polymer matrix. Such behavior aligns with reports on thermally

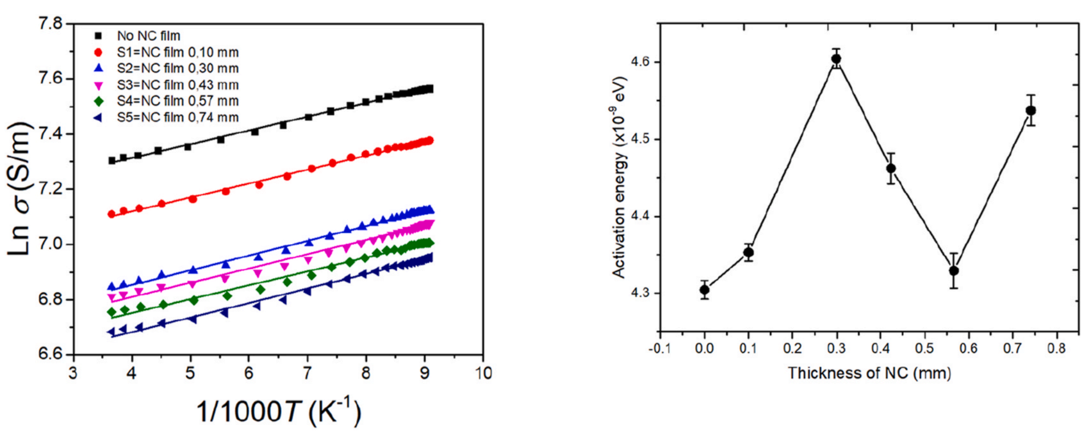

(a) (b)

Fig. 7. (a) Curve of ln σ vs. $1/1000T$ for Cu/Ni/NC and (b) Activation energy on the various NC coating thicknesses.

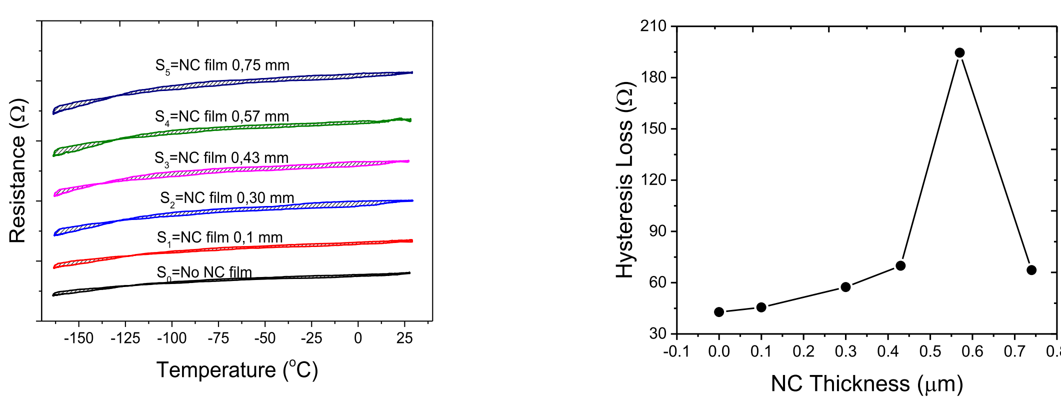

(a) (b)

Fig. 8. (a) The resistance–temperature characteristics of Cu/Ni sensors coated with various thicknesses of NC, and (b) Effect of NC thickness on hysteresis behavior.

cycled polymer systems, where viscoelastic and relaxation effects intensify in thicker films [53], [54].

Interestingly, when the thickness was increased to 0.74 mm, the hysteresis loss decreased, although it remained higher than that of thinner coatings. This reduction is likely attributable to internal heat redistribution or saturation of viscoelastic relaxation, leading to more uniform yet slower thermal diffusion. A comparable trend has been observed in organic dielectric films under cyclic thermal stress, where charge redistribution and structural rearrangements approach a semi-equilibrium state beyond a critical threshold [55].

These findings confirm that the NC layer thickness is a critical factor governing the thermal hysteresis behavior of Cu/Ni sensors. Thin layers provide effective mechanical protection with minimal impact on dynamic performance, whereas excessive thickness induces nonlinear thermal effects and hysteresis-related inaccuracies. An optimal balance between thermal stability and sensor responsiveness is achieved at 0.30–0.43 mm, beyond which performance degrades.

3.7. Effect of NC thickness on the sensor's response to temperature

Fig. 9 shows the resistance–temperature relationship for samples with varying NC layer thicknesses. All samples exhibit a positive resistance–temperature correlation, consistent with metallic behavior, in which higher temperatures enhance phonon–electron interactions, thereby increasing electrical resistance [56].

The reference sample without an NC layer (S0) exhibits the lowest baseline resistance, approximately 850 Ω at −160 °C, increasing to about 1150 Ω at 0 °C. In contrast, NC-coated samples show a progressive rise in baseline resistance with increasing coating thickness. For example, the S5 sample with a 0.74 mm NC layer shows ∼1500 Ω at −160 °C and ∼1850 Ω at 0 °C. This trend indicates that the NC layer adds resistive properties, likely due to its intrinsic insulating behavior and enhanced interfacial scattering effects [57].

3.8. Effect of NC thickness on enhanced thermal sensitivity of Cu/Ni/NC sensors

Fig. 10 illustrates the absolute sensitivity of Cu/Ni/NC sensors with varying NC layer thicknesses under cryogenic conditions.

Incorporating an NC layer significantly affects thermal sensitivity, particularly at ultra-low temperatures. The data reveal a nonlinear increase in sensitivity with thicker NC layers, notably at −150 °C and −175 °C, where S5 exceeds 7 Ω/°C [58], [59]. This behavior is likely due to changes in the dielectric constant and thermal retention properties of NC at low temperatures [60]. A threshold near 0.30 mm separates a low-sensitivity region from a high-sensitivity region. In contrast, at moderate sub-zero temperatures (e.g., −25 °C), sensitivity decreases, possibly due to NC's insulating nature, which limits thermal diffusion [61].

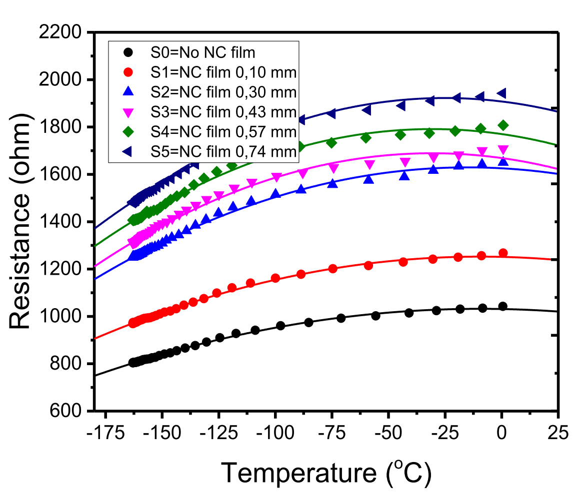

Fig. 9. Resistance-Temperature characteristics of Cu/Ni Coil Sensors.

Sensors coated with thicker NC layers (S4 and S5) demonstrated the highest absolute sensitivity at ultra-low temperatures, exceeding 6 Ω/°C at −160 °C. However, these sensors also exhibited a steeper decline in sensitivity with increasing temperature than those with thinner coatings. Notably, the absolute sensitivity curves intersect at specific temperatures, as summarized in Table 2. These intersection points indicate that, at certain temperatures, Cu/Ni/NC sensors with different NC thicknesses yield identical absolute sensitivity. At such points, the film thickness ceases to serve as a differentiating factor. Before and after these intersections, the relative performance of the sensors reverses. For instance, below −100 °C, sensor S5 outperforms S1 and S2 in terms of sensitivity. Yet above −50 °C, the sensitivity of S5 drops below that of sensors with thinner NC layers. This phenomenon suggests that increasing the thickness of the NC layer enhances sensitivity primarily at cryogenic temperatures. At elevated temperatures, however, sensors with thicker coatings tend to exhibit a more pronounced performance degradation. This behavior may be attributed to structural changes in the polymeric NC layer, which could diminish thermal conductivity, or to variations in dielectric properties with film thickness [62–64].

The results presented in Fig. 8b and summarized in Table 3 show that sensors with different NC layer thicknesses can exhibit identical absolute sensitivity at specific temperatures, as indicated by the intersection points of the sensitivity curves. These intersections occur, for example, at approximately −86 °C for the S4–S2 pair (2.50 Ω/°C) and −57 °C for the S3–S1 pair (1.14 Ω/°C). At these temperatures, the influence of NC thickness on sensitivity becomes negligible, meaning that sensors with different coating thicknesses can deliver equivalent temperature responses [7]. From a practical perspective, these intersection temperatures provide useful criteria for selecting sensor configurations. When the operating temperature of a system lies close to one of these intersection points, multiple sensor designs can achieve nearly identical sensitivity. Therefore, the sensor can be chosen based on other practical considerations such as coating durability, resistance to cryogenic environmental stresses, and fabrication simplicity rather than sensitivity alone.

The presence of these intersections also offers opportunities for fabrication and cost optimization. If comparable sensitivity can be achieved at a given temperature using several NC thicknesses, thinner coatings may be preferred because they generally require shorter deposition time, lower material consumption, and reduced risk of defects such as cracking or delamination during thermal cycling [14]. Conversely, thicker NC layers remain advantageous in applications requiring higher sensitivity at extremely low temperatures, as demonstrated by the superior cryogenic performance of sensors such as S5.

Physically, the occurrence of these intersection points can be attributed to the competing effects of thermal retention and heat transfer resistance in the NC coating. Thicker NC layers enhance thermal retention, which increases sensitivity at very low temperatures. However, they also introduce higher thermal resistance that can limit heat transfer between the environment and the sensing layer at higher temperatures. As a result, the sensitivity curves of sensors with different coating thicknesses intersect at particular temperatures [7], [65].

Overall, the analysis of these intersection points provides practical guidelines for selecting the optimal NC coating thickness according to the intended operating temperature range, enabling a balanced consideration of sensitivity performance, mechanical reliability, and fabrication efficiency.

4. Predictive model for sensitivity

To clarify the physical processes governing the sensor behavior, a schematic illustration of the working mechanism of the Cu/Ni/NC cryogenic temperature sensor is presented in Fig. 11. The NC protective

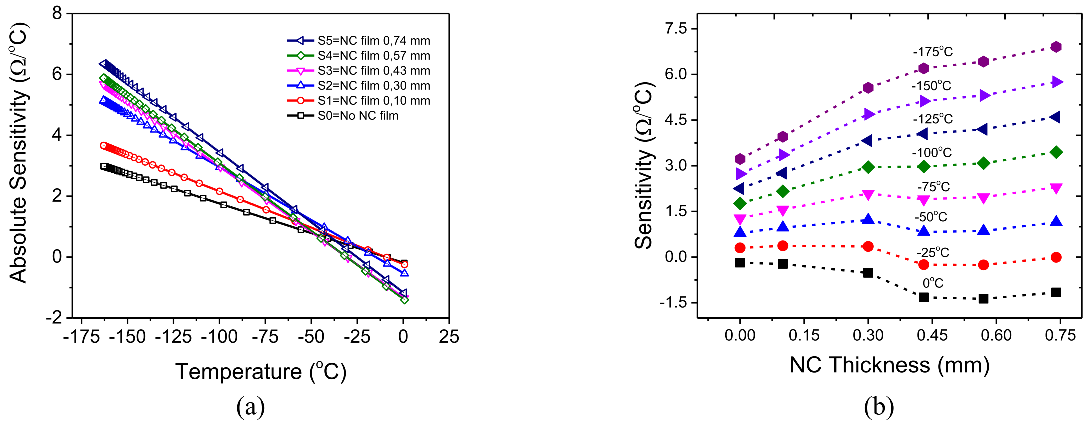

Fig. 10. (a) The absolute temperature sensitivity of Cu/Ni-based sensors coated with NC films of various thicknesses, and (b) A nonlinear increase in sensitivity with thicker NC layers.

Table 2
Fitting constants of absolute sensitivity at various temperatures.

Curve	Slope (Ω/°C^2)	Intercept (Ω/°C)	Physical Meaning
S0	−0.01946 ± 1.46166E-18	−0.18364 ± 2.03406E-16	low sensitive
S1	−0.02388 ± 2.89156E-18	−0.2263 ± 4.14687E-16	moderate sensitive
S2	−0.03474 ± 6.08553E-18	−0.51969 ± 8.96943E-16	moderate-high sensitive
S3	−0.04296 ± 9.25734E-18	−1.32118 ± 1.3580E-15	high sensitive
S4	−0.04452 ± 1.92309E-18	−1.36898 ± 2.73998E-16	very high sensitive
S5	−0.04608 ± 4.23243E-18	−1.16011 ± 5.96891E-16	most sensitive

Table 3
Temperature and absolute sensitivity at the intersection points of two sensor curves.

Curve pair	Intersection Temperature (°C)	Absolute Sensitivity (Ω/°C)	Film Thickness Description
S5 & S4	134	−7.33	Thick vs. medium-thick films
S4 & S2	−86	2.50	Medium vs. thin films
S3 & S1	−57	1.14	Intermediate vs. very thin films
S1 & S0	−10	−0.46	Thinnest film vs. no NC layer
S2 & S0	−21	0.24	Thin film vs. no NC layer

layer modifies heat transfer and interfacial transport, which in turn influences the response time, activation energy, and voltage response of the sensor.

To quantitatively assess the relationship between sensitivity and the physical parameters governing Cu/Ni-based cryogenic temperature sensors, a multivariate logarithmic regression model was developed. The logarithmic formulation was adopted because many transport processes in thermal and electronic systems exhibit power-law scaling. Expressing the model in logarithmic form linearizes the multiplicative dependence between variables and enables quantification of the relative influence of each parameter through the fitted exponents, which describe how thermal dynamics, charge-transport barriers, and interfacial effects collectively influence the sensor sensitivity [66], [67]. In the sensitivity model of the Cu/Ni/NC cryogenic temperature sensor, the parameters used to predict the absolute thermal sensitivity (S) at

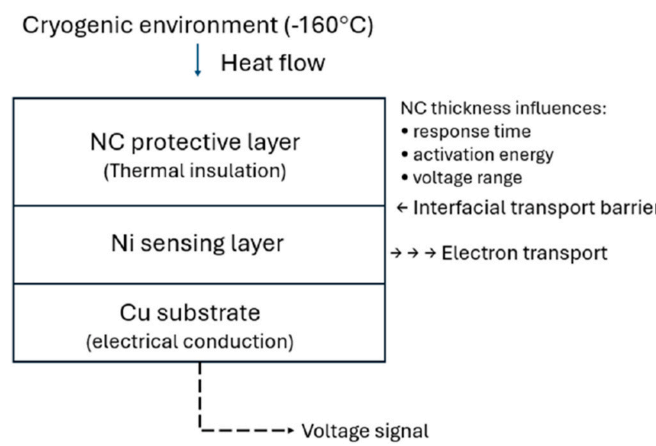

Fig. 11. Schematic diagram of the working mechanism of the Cu/Ni/NC cryogenic temperature sensor.

−150 °C reflect distinct physical mechanisms governing the sensor response. The response time (t_r) characterizes the thermal dynamics of the sensor; a larger t_r indicates slower thermal equilibration due to higher thermal resistance. The activation energy (E_a) represents the energy barrier for electron transport in the Cu/Ni film, where higher E_a values indicate a stronger temperature dependence of the electrical conduction. The hysteresis loss (HL) is associated with the sensor's stability during cooling–heating cycles, with higher values indicating greater differences between the two processes. The nitrocellulose coating thickness (w_{NC}) controls the thermal resistance between the sensing layer and the surrounding environment, where increasing w_{NC} generally enhances the temperature gradient across the sensor. Meanwhile, the voltage range (ΔV) represents the electrical signal variation induced by temperature changes and reflects the magnitude of the sensor's electrical response under cryogenic conditions. The experimental parameters used in the regression model are summarized in Table 4.

The empirical model is expressed in logarithmic form as

$$\ln S = p + q\ln t_r + r\ln E_a + s\ln H_L + u\ln \Delta V + z\ln w_{\mathrm{NC}} \quad (11)$$

which can be equivalently expressed in exponential form as:

$$S = K\frac{t_r^q E_a^r H_L^s w_{NC}^z}{(\Delta V)^u} \quad (12)$$

where p is the logarithmic intercept, $K = e^p$, and q, r, s, u, and z are the regression exponents describing the relative influence of each

Table 4
Experimental parameters used in the sensitivity regression model.

Label	NC Thickness (mm)	t_r (s)	E_a (eV)	H_L (Ohm)	ΔV (V)	w_{NC} (mm)	S_{exp} (Ω/°C)	S_{model} (Ω/°C)	Relative Error
S0	0.00	277	0.18	0.012	0.13	0.00	0.46	0.52	13.0%
S1	0.10	289	0.22	0.018	0.15	0.10	1.14	1.25	9.6%
S2	0.30	308	0.35	0.025	0.17	0.30	2.50	2.61	4.4%
S3	0.43	298	0.32	0.035	0.14	0.43	4.00	4.15	3.8%
S4	0.57	290	0.28	0.057	0.11	0.57	6.50	6.30	3.1%
S5	0.74	284	0.26	0.045	0.10	0.74	7.20	7.45	3.5%

parameter.

Although the regression model is empirical, the selected parameters are physically linked to the governing processes of the sensor, including heat transfer through the NC coating, charge transport within the Cu/Ni sensing layer, and interfacial effects between the metal film and the polymer coating. Therefore, the fitted exponents provide a phenomenological description of how these physical processes collectively influence the sensor's temperature sensitivity.

Table 4 shows that the experimentally measured sensitivity increases significantly with increasing NC coating thickness, from 0.46 Ω/°C for the uncoated sensor (S0) to 7.20 Ω/°C for the thickest coating (S5). This trend indicates that the NC layer enhances the sensor response under cryogenic conditions, most likely by modifying heat transfer and interfacial transport mechanisms. The activation energy also increases from 0.18 eV to 0.35 eV at intermediate coating thicknesses, then slightly decreases for thicker coatings, suggesting that the polymer layer modifies the energy barrier for charge transport. Meanwhile, the response time varies within a relatively narrow range (277–308 s), indicating comparable thermal equilibration dynamics across the samples.

The fitted constants $p, K, q, r, s, u,$ and z are −1.457, 0.223, 0.90, 1.10, 0.20, 1, and 0.25, respectively. The negative value of p corresponds to the logarithmic intercept of the regression equation and represents the baseline scaling constant of the model. The regression exponents provide insight into the relative influence of each parameter. The largest exponent corresponds to the activation energy ($r = 1.10$), indicating that the charge-transport barrier likely plays a dominant role in determining the temperature dependence of electrical conductivity and therefore strongly influences the sensor sensitivity. The response time exponent ($q = 0.90$) is also relatively large, suggesting that slower thermal equilibration—associated with stronger thermal insulation, can enhance the measurable resistance change.

In contrast, hysteresis loss exhibits a smaller exponent ($s = 0.20$), implying that thermal lag contributes only moderately to the overall sensitivity. The exponent associated with the voltage range ($u \approx 1$) indicates an approximately linear relationship between the electrical response amplitude and sensitivity. Finally, the exponent associated with the NC coating thickness ($z = 0.25$) suggests that the polymer layer primarily acts as a secondary structural modifier, influencing heat transfer and interfacial charge transport rather than being the dominant factor controlling sensitivity.

To evaluate the predictive capability of the model, the calculated sensitivities were compared with the experimentally measured values at −150 °C, as shown in Fig. 12. The results demonstrate good agreement between the experimental and predicted values, with relative errors below approximately 13%, indicating that the regression model captures the main physical trends governing the sensor response. Because the number of experimental samples is limited, the regression model should be regarded as an empirical correlation rather than a universal predictive law. Nevertheless, the model provides useful insight into the relative influence of the key physical parameters governing the sensitivity of Cu/Ni/NC cryogenic sensors.

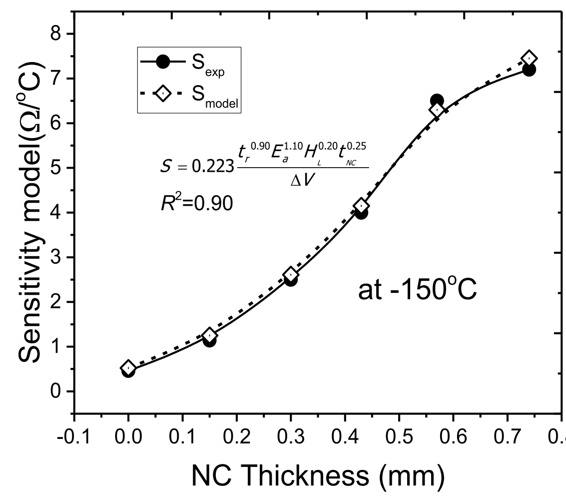

Fig. 12. Comparison between experimental and predicted sensitivity of Cu/Ni/NC sensors at −150 °C.

5. Conclusion

This study demonstrates that the thickness of nitrocellulose (NC) coatings has a pronounced impact on the thermal and electrical characteristics of Cu/Ni-based cryogenic sensors. Increasing NC thickness initially prolongs the response time due to enhanced thermal insulation, with optimal performance achieved at 0.30–0.43 mm, where the voltage range peaks and activation energy is maximized. Thinner or thicker layers permit partial conduction, while hysteresis loss—indicative of thermal lag—is greatest at 0.57 mm, suggesting excessive heat retention. Coatings thicker than 0.43 mm enhance cryogenic sensitivity but compromise response speed and reversibility. A multivariate logarithmic regression model incorporating NC thickness accurately captures nonlinear sensitivity behavior, providing a robust predictive framework. These findings offer practical guidelines for tailoring NC layer thickness to achieve an optimal balance between sensitivity, stability, and operational reliability in extreme low-temperature environments.

Declaration of AI using assisted technologies

AI tools were used to assist in language editing and proofreading, but the authors are fully responsible for the content.

Funding

This research was funded by the Ministry of Research, Technology, and Higher Education of the Republic of Indonesia (Kemenristekdikti), which funded this work through the master's Thesis Grant, under Decree No. 107/E5/PG.02.00.PL/2024 and Agreement/Contract No. 083/PTM/LPPM-UAD/VI/2024.

CRediT authorship contribution statement

Moh Toifur: Conceptualization, Data curation, Formal analysis, Validation, Visualization, Writing – original draft. **Yazid Yaakob:** Investigation, Writing – review & editing. **Okimustava:** Methodology, Project administration. **Azmi Khusnani:** Data curation, Writing – review & editing. **Adi Jufriansah:** Writing – review & editing. **Eko Susanto:** Data curation.

Declaration of competing interest

The authors declare the following financial interests/personal relationships which may be considered as potential competing interests: Moh Toifur reports financial support was provided by National Research and Innovation Agency Republic of Indonesia. If there are other authors, they declare that they have no known competing financial interests or personal relationships that could have appeared to influence the work reported in this paper.

Acknowledgment

The author would like to thank the Ministry of Research, Technology, and Higher Education of the Republic of Indonesia (Kemenristekdikti) and the Sensor and Transducer Laboratory of Universitas Ahmad Dahlan.

Data availability

The data are available from the corresponding author upon reasonable request.

References

[1] Y. Zhao, W. Ji, L. Chen, J. Guo, J. Wang, Effect of cryogenic freezing combined with precooling on freezing rates and the quality of golden pomfret (Trachinotus ovatus), J. Food Process. Eng. 42 (8) (Dec. 2019), https://doi.org/10.1111/jfpe.13296.
[2] M. Sharafi, S.M. Borghei-Rad, M. Hezavehei, A. Shahverdi, J.D. Benson, Cryopreservation of semen in domestic animals: a review of current challenges, applications, and prospective strategies, Animals 12 (23) (Nov. 2022) 3271, https://doi.org/10.3390/ani12233271.
[3] G. Wang, J. Li, Y. Liu, L. Wei, C. Shi, G. Hong, Design and test of a liquid helium cryostat with automatic level control for cooling a superconductive single-flux-quantum circuit chip, Cryogenics 124 (Jun. 2022) 103467, https://doi.org/10.1016/j.cryogenics.2022.103467.
[4] A. Arav, Cryopreservation by directional freezing and vitrification focusing on large tissues and organs, Cells 11 (7) (Mar. 2022) 1072, https://doi.org/10.3390/cells11071072.
[5] W. Hong, S. Shen, Z. Wang, Z. Wang, W. Cai, A cryogenic sensor based on fiber bragg grating for storage monitoring of liquefied natural gas, Cryogenics 97 (Jan. 2019) 7–12, https://doi.org/10.1016/j.cryogenics.2018.11.001.
[6] G.T. Jung, et al., Lipidomic changes in mouse oocytes vitrified in PEG 8000-supplemented vitrification solutions, Cryobiology 99 (Apr. 2021) 140–148, https://doi.org/10.1016/j.cryobiol.2020.11.004.
[7] M. Cai, et al., Enhanced cryogenic temperature sensor from 320 to 20 K amplified by vernier effect, APL Photonics 10 (3) (Mar. 2025), https://doi.org/10.1063/5.0247962.
[8] M. Koo, et al., Distance computation based on coupled spin-torque oscillators: application to image processing, Phys. Rev. Appl. 14 (3) (Sep. 2020) 034001, https://doi.org/10.1103/PhysRevApplied.14.034001.
[9] K. Liu, et al., Deep cryogenic treatment characteristics of a deformation-processed cu-ni-co-si alloy, Materials 15 (9) (Apr. 2022) 3051, https://doi.org/10.3390/ma15093051.
[10] A. Nespoli, et al., A study of a cryogenic CuAlMn shape memory alloy, Metals 14 (3) (Mar. 2024) 323, https://doi.org/10.3390/met14030323.
[11] I.I. Tumkin, E.M. Khairullina, M.S. Panov, K. Yoshidomi, M. Mizoshiri, Copper and nickel microsensors produced by selective laser reductive sintering for non-enzymatic glucose detection, Materials 14 (10) (May 2021) 2493, https://doi.org/10.3390/ma14102493.
[12] S.-C. Kwon, M.-S. Jo, D.-H. Ko, H.-U. Oh, Viscoelastic multilayered blade-type passive vibration isolation system for a spaceborne cryogenic cooler, Cryogenics 105 (Jan. 2020) 102982, https://doi.org/10.1016/j.cryogenics.2019.102982.
[13] H. Saini, S. Gangwar, C.S. Yadav, M.S. Khatri, Synthesis and characterization of Cu-Ni thin films at different pH baths: a comparative study using XRD, XPS and corrosion analysis, J. Phys. Conf. Ser. 2663 (1) (Dec. 2023) 012011, https://doi.org/10.1088/1742-6596/2663/1/012011.
[14] D. Mahana, A.K. Mauraya, P. Singh, S.K. Muthusamy, Evolution of CuO thin films through thermal oxidation of Cu films prepared by physical vapour deposition techniques, Solid State Commun. 366–367 (Jun. 2023) 115152, https://doi.org/10.1016/j.ssc.2023.115152.
[15] A. Benatmane, H. Dhiflaoui, M. Ewald, H. Benhayoune, A. EL Hdiy, Heat treatment effects on the microstructural and mechanical properties of electrodeposited Cu-Ni coatings, J. Mater. Eng. Perform. 34 (16) (Aug. 2025) 18260–18276, https://doi.org/10.1007/s11665-024-10500-y.
[16] Y. Li, F. Zeng, B. Gao, H. Chen, F. Zhang, Y. Gu, Durable anti-oxidation mechanism and failure analysis of the ZrSiO4 compound glass coating for carbon/carbon composites, Surf. Coat. Technol. 349 (Sep. 2018) 233–241, https://doi.org/10.1016/j.surfcoat.2018.05.050.
[17] W. Ge, W. Gao, Y. Tian, P. Zhang, J. Zhu, Y. Li, Tunable dual-mode photoluminescences from SrAl2O4: Eu/Yb nanofibers by different atmospheric annealing, J. Alloys Compd. 859 (Apr. 2021) 158261, https://doi.org/10.1016/j.jallcom.2020.158261.
[18] S.A.A. Fuzi, M. H. Hj Jumali, B.A. Al-Asbahi, S.M.H. Qaid, Photophysical and energy transfer mechanism studies of poly (9,9-di-n-octylflourenyl-2,7-diyl)/Fluorol 7GA/Poly [2-methoxy-5-(2-ethylhexyloxy)-1,4-phenylenevinylene] ternary organic blend films, Thin Solid Films 683 (Aug. 2019) 90–96, https://doi.org/10.1016/j.tsf.2019.05.022.
[19] L. Shao, et al., Combustion behaviour and mechanism of TC4 and TC11 alloys, Corros. Sci. 168 (May 2020) 108564, https://doi.org/10.1016/j.corsci.2020.108564.
[20] R. Kotipalli, R. Delamare, O. Poncelet, X. Tang, L.A. Francis, D. Flandre, Passivation effects of atomic-layer-deposited aluminum oxide, EPJ Photovoltaics 4 (Sep. 2013) 45107, https://doi.org/10.1051/epjpv/2013023.
[21] W. Burgstaller, M. Hafner, M. Voith, A.I. Mardare, A.W. Hassel, Copper–nickel oxide thin film library reactively co-sputtered from a metallic sectioned cathode, J. Mater. Res. 29 (1) (Jan. 2014) 148–157, https://doi.org/10.1557/jmr.2013.336.
[22] C. Martínez, B. Valverde, A. Del Valle-Rodríguez, B. Bustos-De La Fuente, I. F. Machado, F. Briones, Analysis of the wear and corrosion resistance on cu-ni-al composites reinforced with CeO2 nanoparticles, Materials 18 (11) (May 2025) 2438, https://doi.org/10.3390/ma18112438.
[23] T.T. Salunkhe, D.J. Lee, H.K. Lee, H.W. Choi, S.J. Park, I.T. Kim, Enhancing temperature sensitivity of the fabry–perot interferometer sensor with optimization of the coating thickness of polystyrene, Sensors 20 (3) (Jan. 2020) 794, https://doi.org/10.3390/s20030794.
[24] Suprapto, et al., Effect of ITO poling thickness, temperature, and protective layer on piezoelectric PVDF films, Mater. Sci. Semicond. Process. 174 (May 2024) 108156, https://doi.org/10.1016/j.mssp.2024.108156.
[25] B.H. Kang, et al., Improvement of the stability and optoelectronic characteristics of molybdenum disulfide thin-film transistors by applying a nitrocellulose passivation layer, J. Informat. Displ. 21 (2) (Apr. 2020) 123–130, https://doi.org/10.1080/15980316.2019.1710585.
[26] A. Pazzaglia, A. Maffini, D. Dellasega, A. Lamperti, M. Passoni, Reference-free evaluation of thin films mass thickness and composition through energy dispersive X-ray spectroscopy, Mater. Charact. 153 (Jul. 2019) 92–102, https://doi.org/10.1016/j.matchar.2019.04.030.
[27] L. Liu, et al., Recent advances in flexible temperature sensors: materials, mechanism, fabrication, and applications, Adv. Sci. 11 (36) (Sep. 2024), https://doi.org/10.1002/advs.202405003.
[28] S. Wang, S. Zhu, Impact source localization and vibration intensity prediction on construction sites, Measurement 175 (Apr. 2021) 109148, https://doi.org/10.1016/j.measurement.2021.109148.
[29] X. Hou, B. Xiong, Y. Wang, L. Wang, H. Wang, Determination of trace lead and cadmium in decorative material using disposable screen-printed electrode electrically modified with reduced graphene Oxide/L-Cysteine/Bi-Film, Sensors 20 (5) (Feb. 2020) 1322, https://doi.org/10.3390/s20051322.
[30] C. Naumann, T. Carlesi, H. Otto, C. Cierpka, D. Laboureur, Dynamic characterization of fiber bragg grating temperature sensors, Exp. Therm. Fluid Sci. 156 (Jul. 2024) 111222, https://doi.org/10.1016/j.expthermflusci.2024.111222.
[31] M.H. Wang, Y. Sui, W.N. Zhou, X. An, W. Dong, AIoT enabled resampling filter for temperature extraction of the brillouin gain spectrum, Opt. Express 30 (20) (Sep. 2022) 36110, https://doi.org/10.1364/OE.465460.
[32] V.I. Chasnyk, D.V. Chasnyk, O.M. Kaidash, Activation energy of electrical conductivity and characteristics of microwave radiation absorption in AlN–SiC composite, J. Superhard Mater. 46 (4) (Aug. 2024) 285–292, https://doi.org/10.3103/S1063457624040026.
[33] A.A. Aljubouri, A.D. Faisal, W.K. Khalef, Fabrication of temperature sensor based on copper oxide nanowires grown on titanium coated glass substrate, Mater. Sci. Pol. 36 (3) (Sep. 2018) 460–468, https://doi.org/10.2478/msp-2018-0051.
[34] L.H. Namisnak, S. Khoshnevis, K.R. Diller, A conformable two-dimensional resistance temperature detector for measuring average skin temperature, J. Med. Device. 15 (3) (Sep. 2021), https://doi.org/10.1115/1.4051442.
[35] S. Grasso, et al., BIONOTE as an innovative biosensor for measuring endocannabinoid levels, Sensors 21 (2) (Jan. 2021) 489, https://doi.org/10.3390/s21020489.
[36] F. Le Goupil, G. Payrot, S. Khiev, W. Smaal, G. Hadziioannou, Fully printed sensors for in situ temperature, heat flow, and thermal conductivity measurements in flexible devices, ACS Omega 8 (9) (Mar. 2023) 8481–8487, https://doi.org/10.1021/acsomega.2c07590.
[37] C.T. Harris, T.-M. Lu, A PtNiGe resistance thermometer for cryogenic applications, Rev. Sci. Instrum. 92 (5) (May 2021), https://doi.org/10.1063/5.0014007.
[38] A.-T. Buruiana, et al., Micrometer sized hexagonal chromium selenide flakes for cryogenic temperature sensors, Sensors 21 (23) (Dec. 2021) 8084, https://doi.org/10.3390/s21238084.
[39] D. Setiamukti, A. Khusnani, Moh Toifur, The effect of electrolyte concentration on the sensitivity of low-temperature sensor performance of Cu/Ni film, Sc. Technol. Indon. 5 (2) (Apr. 2020) 28, https://doi.org/10.26554/sti.2020.5.2.28-33.

[40] D. Chen, et al., A review of the polymer for cryogenic application: methods, mechanisms and perspectives, Polymers 13 (3) (Jan. 2021) 320, https://doi.org/10.3390/polym13030320.
[41] Y. Ren, H. Song, Q. Cai, Z. Cai, Y. Liu, B. Wang, Modeling analysis and experimental study on epoxy packaged FBG sensor for cryogenic temperature measurement, Opt. Fiber Technol. 84 (May 2024) 103710, https://doi.org/10.1016/j.yofte.2024.103710.
[42] Moh Toifur, M.L. Khansa, Okimustava, A. Khusnani, Ridwan, The effect of deposition time on the voltage range and sensitivity of Cu/Ni as low-temperature sensor resulted from electroplating assisted by a transverse magnetic field, Key Eng. Mater. 855 (Jul. 2020) 185–190. https://doi.org/10.4028/www.scientific.net/KEM.855.185.
[43] W. Li, et al., Microsecond-scale transient thermal sensing enabled by flexible Mo1−xWxS2 alloys, Research 7 (Jan. 2024), https://doi.org/10.34133/research.0452.
[44] S. Cesnik, G. Hernández Rodríguez, A. Bergmann, A.M. Coclite, Ultrafast humidity sensing layers made by two-photon polymerization and initiated chemical vapor deposition, Adv. Sens. Res. 2 (10) (Oct. 2023), https://doi.org/10.1002/adsr.202200100.
[45] B. Sochor, et al., Effect of layer thickness on the thermoelectric properties of fully sprayed poly(3-hexylthiophene-2,5-diyl) thin films doped with chloroauric acid, J. Coat. Technol. Res. 21 (6) (Nov. 2024) 1945–1954, https://doi.org/10.1007/s11998-024-01008-0.
[46] Y.-L. Shen, M.G. Abdo, I.J. Van Rooyen, Thermal conductivity of crack-containing media: a numerical study, J. Compos. Mater. 56 (16) (Jul. 2022) 2495–2508, https://doi.org/10.1177/00219983221095502.
[47] U. Sampath, M. Song, Epoxy-coated side-polished fiber-optic temperature sensor for cryogenic conditions, Sensors 23 (5) (Mar. 2023) 2850, https://doi.org/10.3390/s23052850.
[48] T. Chowdhury, N. D'Souza, N. Dahotre, Low-cost reliable corrosion sensors using ZnO-PVDF nanocomposite textiles, Sensors 21 (12) (Jun. 2021) 4147, https://doi.org/10.3390/s21124147.
[49] S.-Y. Chu, M.-J. Wu, T.-H. Yeh, C.-T. Lee, H.-Y. Lee, Investigation of high-sensitivity NO2 gas sensors with Ga2O3 nanorod sensing membrane grown by hydrothermal synthesis method, Nanomaterials 13 (6) (Mar. 2023) 1064, https://doi.org/10.3390/nano13061064.
[50] M.A. Kudryashov, et al., Hopping conductivity and dielectric relaxations in Ag/PAN nanocomposites, Polymers 13 (19) (Sep. 2021) 3251, https://doi.org/10.3390/polym13193251.
[51] M. Michelazzi, D. Fabiani, Electrical conduction in thin-film polypropylene capacitors, Energies 16 (18) (Sep. 2023) 6631, https://doi.org/10.3390/en16186631.
[52] H. Sun, et al., Graphene-based dual-function acoustic transducers for machine learning-assisted human–robot interfaces, InfoMat 5 (2) (Feb. 2023), https://doi.org/10.1002/inf2.12385.
[53] A. Ebrahimi, J. Scott, K. Ghorbani, Microwave reflective biosensor for glucose level detection in aqueous solutions, Sens. Actuators A Phys. 301 (Jan. 2020) 111662, https://doi.org/10.1016/j.sna.2019.111662.
[54] L. Tong, G. Yang, X. Lei, Y. You, X. Liu, Improving the thermal and mechanical properties of poly(arylene ether nitrile) films through blending high- and low-molecular-weight polymers, J. Appl. Polym. Sci. 137 (11) (Mar. 2020), https://doi.org/10.1002/app.48457.
[55] J. Singh, R.G. Singh, S.K. Gautam, H. Gupta, F. Singh, A versatile multifaceted resistive switching memory activated by light and ion irradiation in poly (3-octylthiophene)-zinc oxide hybrids, Org. Electron. 87 (Dec. 2020) 105932, https://doi.org/10.1016/j.orgel.2020.105932.
[56] W. Wei, Y. Yi, J. Song, X. Chen, J. Li, J. Li, Tunable graphene/nitrocellulose temperature alarm sensors, ACS Appl. Mater. Interfaces 14 (11) (Mar. 2022) 13790–13800, https://doi.org/10.1021/acsami.2c02340.
[57] X. Nian, Q. Xie, X. Kong, Y. Yao, K. Huang, Experimental and numerical study on protective effect of RC blast wall against air shock wave, Def. Technol. 31 (Jan. 2024) 567–579, https://doi.org/10.1016/j.dt.2022.11.005.
[58] R. Eivazzadeh-Keihan, F. Radinekiyan, H. Madanchi, H.A.M. Aliabadi, A. Maleki, Graphene oxide/alginate/silk fibroin composite as a novel bionanostructure with improved blood compatibility, less toxicity and enhanced mechanical properties, Carbohydr. Polym. 248 (Nov. 2020) 116802, https://doi.org/10.1016/j.carbpol.2020.116802.
[59] G. Wang, Y. Wang, Y. Luo, S. Luo, A self-converted strategy toward multifunctional composites with laser-induced graphitic structures, Compos. Sci. Technol. 199 (Oct. 2020) 108334, https://doi.org/10.1016/j.compscitech.2020.108334.
[60] A. Tulcan, M.D. Vasilescu, L. Tulcan, Comparative study of the influence of bio-resin color on the dimension, flatness and straightness of the part in the 3D printing process, Polymers 13 (9) (Apr. 2021) 1412, https://doi.org/10.3390/polym13091412.
[61] O.V. Ivanov, P. Caldas, G. Rego, High sensitivity cryogenic temperature sensors based on arc-induced long-period fiber gratings, Sensors 22 (19) (Sep. 2022) 7119, https://doi.org/10.3390/s22197119.
[62] W. Du, et al., Temperature-mediated structural evolution of vapor–phase deposited cyclosiloxane polymer thin films for enhanced mechanical properties and thermal conductivity, Int. J. Extrem. Manuf. 5 (2) (Jun. 2023) 025101, https://doi.org/10.1088/2631-7990/acc5c1.
[63] V.H. Tran, J.-D. Kim, J.-H. Kim, S.-K. Kim, J.-M. Lee, Influence of cellulose nanocrystal on the cryogenic mechanical behavior and thermal conductivity of polyurethane composite, J. Polym. Environ. 28 (4) (Apr. 2020) 1169–1179, https://doi.org/10.1007/s10924-020-01673-3.
[64] D. Chen, et al., A review of the polymer for cryogenic application: methods, mechanisms and perspectives, Polymers 13 (3) (Jan. 2021) 320, https://doi.org/10.3390/polym13030320.
[65] B. Liu, V.I. Khvesyuk, A.A. Barinov, M. Wang, Effect of interfacial roughness on thermal boundary conductance: an elastic wave model using the kirchhoff approximation, Int. J. Mech. Sci. 218 (Mar. 2022) 106993, https://doi.org/10.1016/j.ijmecsci.2021.106993.
[66] X. Xie, A. Samaei, J. Guo, W.K. Liu, Z. Gan, Data-driven discovery of dimensionless numbers and governing laws from scarce measurements, Nat. Commun. 13 (1) (Dec. 2022) 7562, https://doi.org/10.1038/s41467-022-35084-w.
[67] J. Song, P. Li, L. Chen, Y. Zhao, F. Tian, B. Li, Scaling law of flow and heat transfer characteristics in turbulent radiative rayleigh-bénard convection of optically thick media, Energies 17 (19) (Oct. 2024) 5009, https://doi.org/10.3390/en17195009.